JACS
JOURNAL OF THE AMERICAN CHEMICAL SOCIETY
pubs.acs.org/JACS
Article

Photoactivation of Boronic Acid Prodrugs via a Phenyl Radical Mechanism: Iridium(III) Anticancer Complex as an Example

Moyi Liu, Yunli Luo, Junyu Yan, Xiaolin Xiong, Xiwen Xing,* Jong Seung Kim,* and Taotao Zou*

Cite This: J. Am. Chem. Soc. 2023, 145, 10082−10091
Read Online

ACCESS | Metrics & More | Article Recommendations | Supporting Information

ABSTRACT: Boronic acid (or ester) is a well-known temporary masking group for developing anticancer prodrugs responsive to tumoral reactive oxygen species (ROS), but their clinic application is largely hampered by the low activation efficiency. Herein, we report a robust photoactivation approach that can spatiotemporally convert boronic acid-caged iridium(III) complex **IrBA** into bioactive **IrNH$_2$** under hypoxic tumor microenvironments. Mechanistic studies show that the phenyl boronic acid moiety in **IrBA** is in equilibrium with phenyl boronate anion that can be photo-oxidized to generate phenyl radical, a highly reactive species that is capable of rapidly capturing O_2 at extremely low concentrations (down to 0.02%). As a result, while **IrBA** could hardly be activated by intrinsic ROS in cancer cells, upon light irradiation, the prodrug is efficiently converted into **IrNH$_2$** even in limited O_2 supply, along with direct damage to mitochondrial DNA and potent antitumor activities in hypoxic 2D monolayer cells, 3D tumor spheroids, and mice bearing tumor xenografts. Of note, the photoactivation approach could be extended to intermolecular photocatalytic activation by external photosensitizers with red absorption and to activate prodrugs of clinic compounds, thus offering a general approach for activation of anticancer organoboron prodrugs.

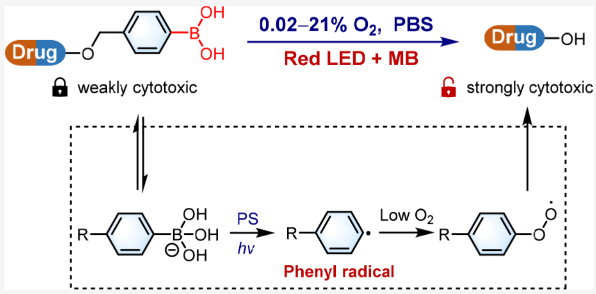

INTRODUCTION

Organoboron (boronic acid/ester) compounds have gained extensive research interest in modern medicinal chemistry.[1−3] Generally, the three-coordinate boron is electron-deficient and can form covalent adducts with biomacromolecules, rendering boron a unique structural role in drug design;[4−6] successful examples include bortezomib, tavaborole, and crisaborole for clinic treatment of different diseases.[7] Of equal significance is the reactivity of organoboron toward certain reactive oxygen species, particularly H_2O_2, which is overexpressed in many types of tumor cells.[8−11] In past years, tremendous efforts have been spent on developing organoboron-based anticancer prodrugs of both organic and inorganic compounds.[12−26] In principle, a majority of bioactive molecules can be created as boronic acid/ester prodrugs based on their hydroxy or amine group that can be functionalized with traceless linkers.[27] These prodrugs can indeed be activated by H_2O_2 and release the intact drug molecules/derivatives (Figure 1a). The bimolecular reaction between phenylboronic acid and H_2O_2 has a relatively slow reaction rate with k_{obs} = 2.4 M^{-1} s^{-1} at pH 7.3.[28] Such a reaction rate suggests that a high concentration of H_2O_2 is required for prodrug activation. However, the endogenous H_2O_2 may not always be sufficient in view of its heterogeneous distribution and the upregulated antioxidant system within tumors.[29] To this end, endeavors to conjugate ROS amplifiers (e.g., ferrocene) or to introduce ROS inducers (e.g., lipopolysaccharide) into boronic prodrugs were found to significantly improve the activation efficiency.[29−33] Nevertheless, it is still of great challenge to develop a spatiotemporally controllable and universal approach for organoboron-prodrug activation.

Photoinduced prodrug activation is one of the most powerful strategies for cancer treatment with spatiotemporal resolution at the disease tissue.[34−37] In the literature, prodrugs based on metal complexes have been rapidly developed owing to their rich photochemical properties.[38,39] Indeed, prodrugs containing metal ions of platinum,[40−47] ruthenium,[48−55] and others[56−62] have been reported that can be either photocatalytically or photochemically activated within localized tumors. In view of the lower side effects for localized cancer treatment as in the clinical photodynamic therapy (PDT), there is a possibility of harnessing surrounding O_2 to aid prodrug activation, such as utilizing the type I photosensitizing mechanism by consuming reductants to photocatalytically reduce O_2 into superoxide radical anion ($O_2^{\bullet-}$) for boron-prodrug activation (Figure 1b).[63,64] However, tumors are known to feature a hypoxic microenvironment with an O_2 content of 0.02−2%.[65] Even though type I PDT has been

Received: January 8, 2023
Published: April 26, 2023

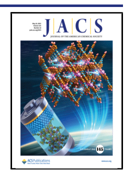

https://doi.org/10.1021/jacs.3c00254
J. Am. Chem. Soc. 2023, 145, 10082−10091

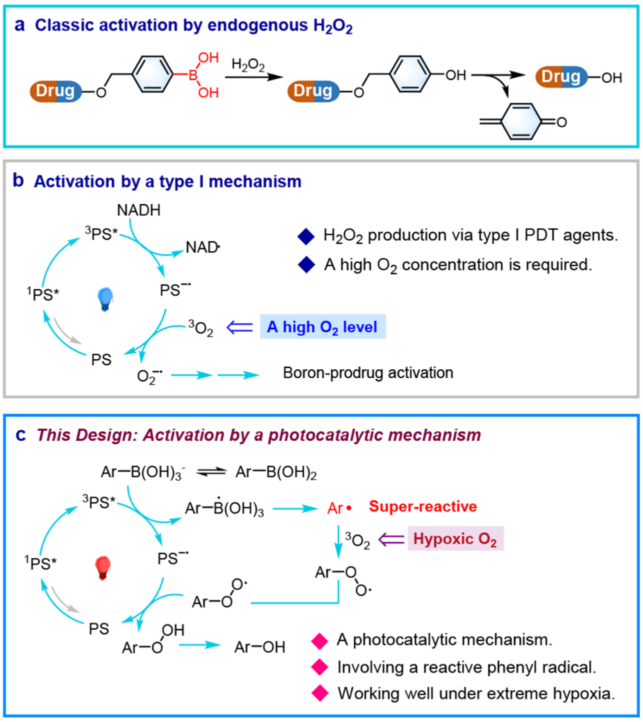

Figure 1. Methods of boronic acid-prodrug activation. (a) Classic activation by endogenous H_2O_2. (b) Activation by a type I photodynamic process needing a high O_2 concentration. (c) The photocatalytic activation in this work that can happen under tumor hypoxia conditions.

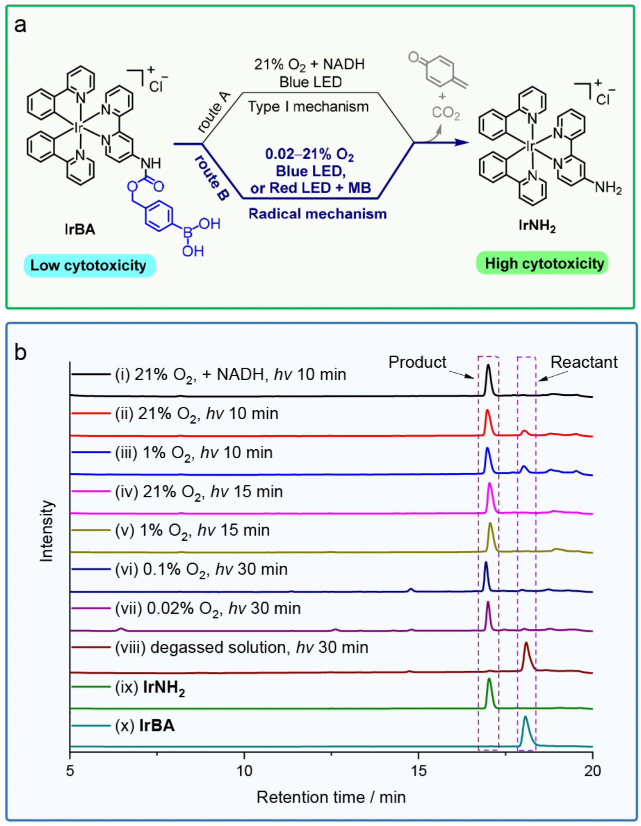

Figure 2. (a) Photoreaction of **IrBA** under different conditions. (b) LC chromatograms for transforming **IrBA** into **IrNH$_2$** in PBS/DMF (8/2, v/v) after 420 nm of irradiation for indicated periods. Intensity is based on $OD_{280\ nm}$.

reported to be less affected by tumor hypoxia, the not-so-strong reaction rate for the photochemically reduced photosensitizer ($PS^{•-}$) to capture O_2 (rate constant $\sim 10^5\ M^{-1} \cdot s^{-1}$)[63] may not provide enough reactive oxygen species (ROS) for boron-prodrug activation (Scheme S1).

In the literature, it has been known that carbon radical is extremely reactive toward dioxygen with a rate constant as high as $\sim 10^9\ M^{-1}\ s^{-1}$;[66,67] thus, even a low concentration of O_2 could trigger fast enough reactions (Scheme S1). In view that boronic acid in aqueous solution is in equilibrium with boronate anion [$R\text{-}B(OH)_3^-$], which can be photocatalytically converted into carbon radical (by directly quenching the excited state of photocatalyst),[68−70] we conceive the possibility of using light to activate boron prodrugs under hypoxic tumor microenvironments via a phenyl carbon radical mechanism (Figure 1c). Based on the fact that organoiridium(III) complexes have well-known photocatalytic properties and many of them are anticancer active,[71−82] we began with a boronic acid-containing Ir(III) complex, **IrBA** (Figure 2a), for a proof-of-concept study. Herein we report that **IrBA** displays a reasonable stability and a low cytotoxicity, but upon light irradiation under hypoxic conditions, the boron moiety can be efficiently removed to generate **IrNH$_2$**, leading to potent antitumor activity in vitro and in vivo. Importantly, such a strategy could be extended to intermolecular photocatalytic activation by external photosensitizers with red absorption and to activate boron-caged clinic drugs. To the best of our knowledge, it is the first time that the photoinduced phenyl radical mechanism was identified to efficiently trigger boron-prodrug activation.

■ RESULTS AND DISCUSSION

Complex **IrBA** was synthesized by refluxing $[Ir(ppy)_2Cl]_2$ (Hppy = 2-phenylpyridine) with a boronic acid-functionalized bipyridine followed by column chromatography for purification. The final product was fully characterized by ^1H NMR, ^{13}C NMR, $^1H-^1H$ COSY, $^1H-^{13}C$ HMBC, $^1H-^{13}C$ HSQC, high-resolution mass spectrometry (HRMS), HPLC, and elemental analysis (see details in the Supporting Information, Figure S1a−d and S2a−c). This complex is soluble in common organic solvents including DMSO, DMF, MeOH, CH_3CN, and CH_2Cl_2. When the complex is dissolved in DMSO as a stock solution (10 mM), it is soluble in water and buffer solution after dilution (≤1% DMSO).

Initially, we tested the stability of **IrBA**. In PBS solution (containing 20% DMF, v/v), the complex did not form new species after 48 h of incubation based on HPLC analysis (Figure S3a). After incubating the complex with the lysate of non-small-cell lung cancer A549 cells for 48 h, HPLC again showed that the complex remained intact (Figure S3b). The stability of **IrBA** in living A549 cells was also examined. After incubating **IrBA** (50 μM) with A549 cells for 48 h, followed by aspiration of medium, washing, cell lysis, and acetone precipitation, over 80% of intact complex in the supernatant was detected (Figure S3c,d). When **IrBA** was incubated with rat liver microsomes, >95% of **IrBA** remained unchanged after 4 h of incubation (Figure S3e), indicating that **IrBA** displays a high metabolic stability.

Next, the photoreactivity of **IrBA** was monitored by HPLC. In the solution of PBS/DMF (8/2, v/v), **IrBA** (20 μM) was

https://doi.org/10.1021/jacs.3c00254
J. Am. Chem. Soc. 2023, 145, 10082−10091

fully converted into **IrNH$_2$** within 10 min of 420 nm light irradiation in the presence of 10 equiv of NADH and under air (21% O_2) as revealed from HPLC analysis (Figure 2b panel i), which is likely caused by the photoinduced superoxide radical anion for boron activation (type I photosensitizing mechanism).

Interestingly, under the same irradiation condition but without NADH, the complex could still be transformed into **IrNH$_2$** in a slightly slower rate with 80% yield in 10 min and ~100% yield in 15 min (Figure 2b panel ii, iv, respectively). Of note, the reaction proceeded equally well under hypoxia (1% O_2) compared to the aerobic condition without NADH, with 78% yield in 10 min and with full conversion within 15 min of 420 nm photoirradiation (Figure 2b panels iii and v). When performing the experiments at extremely low levels of 0.1% O_2 (panel vi) and 0.02% O_2 (panel vii), **IrBA** can still be fully converted into **IrNH$_2$** after 30 min of light irradiation (please note that the typical O_2 concentration in tumors varies from 0.02% to 2% O_2). The non-necessity of external reductants and weak dependence toward O_2 concentrations for the photoconversion of **IrBA** suggest a reaction pathway other than direct O_2 photosensitizing (i.e., not via $O_2^{\bullet-}$). When the reaction solution was bubbled with N_2 or degassed by three cycles of freeze−pump−thaw, no obvious reaction was found (Figure 2b panel viii). Therefore, while the photoreaction is insensitive to O_2 concentration, O_2 is essential for the transformation to occur.

Then we tried to understand the reaction mechanism. As reported before,[83] aromatic boronic acid is a rather weak reductant ($[Ar\text{-}B(OH)_2]^+/[Ar\text{-}B(OH)_2]$ = +2.23 V vs Ag/AgCl (Ar = *p*MeO-CH$_2$-Ph, Figure S4) that is not accessible by most photo-oxidants. However, boronate anion $R\text{-}B(OH)_3^-$, which could be generated from hydrolysis in aqueous solution, is more susceptible to oxidation with a reduction potential of 0.85 V vs Ag/AgCl (Figures 3a, S4). Based on ^1H NMR in the solution of D_2O containing 40 wt % MeOD and 0.1 M NaCl, a pH (adjusted by HCl and NaOH)-dependent chemical shift of the aromatic protons was found (Figure S5a). Plotting the ^1H NMR of protons on the bipyridine ligand versus pH gave a pK_a of 6.76 (Figure S5b). By using ESI-MS, the hydroxylated Ir(III) species was detected with an *m*/*z* of 906.2 in the presence of 1 equiv (full conversion) of $^nBu_4NOH$ (Figure S5c,d). Thus, formation of $R{-}B(OH)_3^-$ exists in an equilibrium ($R{-}B(OH)_3^- + H^+ \leftrightarrow R{-}B(OH)_2 + H_2O$), and the photoreaction could be influenced by pH values. To prove this hypothesis, we performed the photoreaction under different buffer conditions in hypoxia (1% O_2). At pH = 4.5, the reaction was suppressed with 31% yield after 30 min of light irradiation (Figure S6a), which increased to 60% at pH 6.0 (Figure S6b). Instead, at pH 8.0 (10 mM NH_4HCO_3 solution), >99% yield was found within 10 min of photoirradiation (Figure S6b), which is even faster than that in PBS solution (full reaction requiring 15 min). Based on cyclic voltammetry analysis and emission spectrum (Figure S7a,b), the photoexcited Ir806 (a substructure of **IrBA** without the boronic acid moiety) is a good oxidant (reduction potential of 1.02 V) that is able to oxidize $R{-}B(OH)_3^-$ into boric acid and phenyl radical. Indeed, when 1,1-diphenylethene was present, the adducts corresponding to phenyl radical to alkene addition without (*m*/*z* 986.3043) or with (*m*/*z* 984.2929) hydrogen elimination was found under anaerobic conditions based on HRMS analysis (Figures 3b, S8a); moreover, when the radical trapping reagent 2,2,6,6-tetramethylpiperidinyloxy (TEMPO)

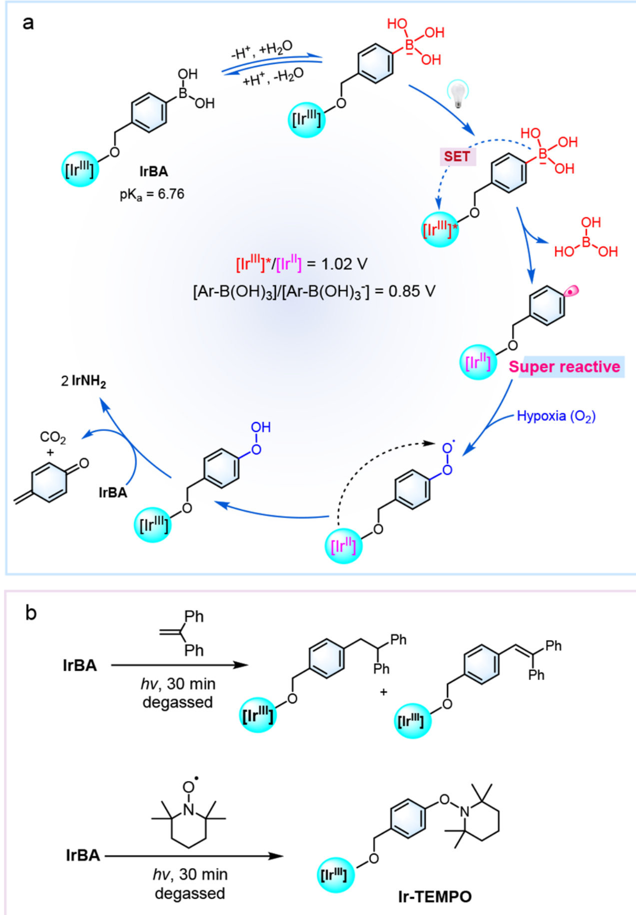

Figure 3. Mechanism studies for photoactivation. (a) A proposed reaction pathway, with the photoredox potentials of the Ir806 and Ar-$B(OH)_3^-$. (b) Photoreaction of **IrBA** with free radical trapping agents.

was present, the product with *m*/*z* (961.3408, error <0.5 ppm) and isotopic pattern consistent with phenyl radical to TEMPO adduct (**Ir-TEMPO**, Figures 3b and S8b) was found, indicating formation of a phenyl radical intermediate. Therefore, the following reaction pathway was proposed (Figure 3a). The boronate anion $R{-}B(OH)_3^-$, generated from hydrolysis in PBS, could be oxidized by the photoexcited Ir(III) intermediate (via single electron transfer, SET) into a strongly reactive phenyl radical, which can capture dioxygen in a fast rate, followed by forming a peroxide species that is capable of oxidizing another molecule of **IrBA** and produce two equivalents of **IrNH$_2$**.

Since the Ir(III) complex is emissive, we then used fluorescence microscopy to monitor the intracellular distribution. After incubating A549 cells with **IrBA** (2 μM) for 4 h, bright green emission was observed in the cytoplasm, which overlaid well with MitoTracker Red with a Pearson's correlation coefficient (PCC) of 0.83 (Figure 4a, upper panel), and it also displayed a good overlap with LysoTracker Red but with a smaller PCC of 0.52 (Figure 4a, lower panel). Since carbon radical is known to directly damage DNA,[84] we considered that the surrounding DNA (possibly from mitochondria) may be destroyed if the above-mentioned photoreaction can happen in cancer cells. To this end, we treated A549 cells with **IrBA** for 4 h, which was subsequently subjected to hypoxia conditions for 1 h (<0.1% O_2)[85] followed

https://doi.org/10.1021/jacs.3c00254
J. Am. Chem. Soc. 2023, 145, 10082−10091

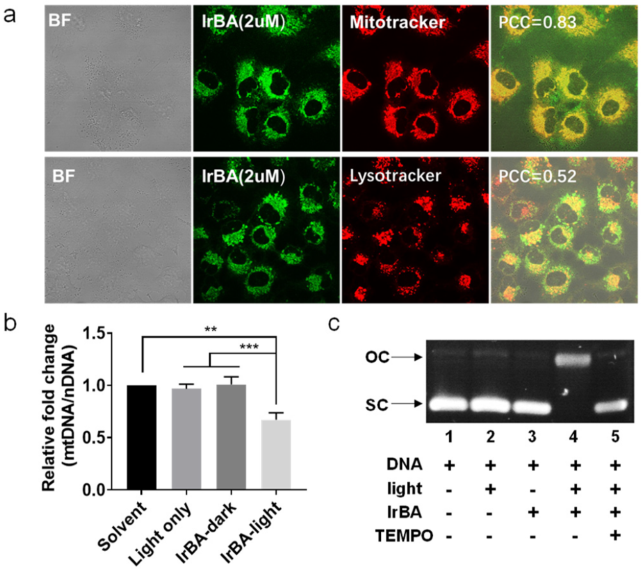

Figure 4. (a) Fluorescence images of **IrBA** (2 μM) in A549 cells. The cells were treated with MitoTracker Red or LysoTracker Red for colocalization analysis. (b) Relative fold change of mtDNA/nDNA after treating A549 cells with **IrBA** with or without 420 nm light irradiation under hypoxia. (c) Gel electrophoresis for the pUC19 plasmid treated with **IrBA** with or without 420 nm light irradiation in hypoxic solution (<0.1% O_2).

by 420 nm irradiation for 10 min. Then, we examined the integrity of mitochondrial DNA (mtDNA) and nuclear DNA (nDNA) by measuring the representative mtDNA $tRNA^{Leu(UUR)}$ and nDNA β2-microglobulin using real-time polymerase chain reaction (qPCR).[86,87] As the results show in Figure 4b, mtDNA in the **IrBA**-light group was damaged to a higher extent compared to nDNA with a fold-ratio of 0.67 ($p < 0.01$), whereas the light-only and **IrBA**-dark groups did not show any change, suggesting that phenyl carbon radical was indeed generated under the cellular environment. In fact, in the solution containing supercoiled (sc) pUC19 plasmid under an atmosphere of <0.1% O_2, the photoactivated **IrBA** directly destroyed the plasmid DNA into open circular (OC) form (Figure 4c); of note, such an activity was fully inhibited in the presence of TEMPO, a radical trapping reagent that can selectively suppress carbon-centered radicals, but not oxygen-centered radicals.[88]

Subsequently, we characterized the photoreaction products in cancer cells. A549 cells were treated with **IrBA** for 4 h and then 420 nm light irradiation for 30 min under hypoxia (<0.1% O_2), followed by aspirating the medium, washing, and cell lysing. HPLC analysis of the supernatant of the cell lysates after acetone precipitation showed >95% conversion into **IrNH$_2$** (Figure S9). For comparison, in the similar condition but without light irradiation, less than 10% conversion was observed. These results collectively revealed that photo-activation is capable of efficiently transforming **IrBA** into **IrNH$_2$** in cancer cells via a phenyl radical mechanism under hypoxic conditions.

Since the cationic Ir(III) complexes accumulated in mitochondria may induce mitochondria depolarization, we monitored the mitochondria membrane potential of A549 cells by JC-1, a cationic dye that displays aggregated orange to red emission in normal mitochondria but shows monomer green color when mitochondria are depolarized. As shown in Figure S10, while only red emission was observed in cells treated with **IrBA** (5 μM) in the dark, intensive green fluorescence but limited red emission was detected when the complex-treated cancer cells were further irradiated with 420 nm light for 10 min under hypoxic conditions, suggesting distinct loss of MMP and consistent with **IrBA** to **IrNH$_2$** transformation in cancer cells. In view that mitochondrial dysfunction may lead to apoptosis, the treated cells were further examined by annexin V/PI dual staining. As shown in Figure S11, **IrBA** induced neither green (annexin V) nor red (PI) fluorescence under dark conditions; after 420 nm irradiation for 10 min, bright green emission with negligible red signals was detected, indicative of early apoptosis. These results collectively indicate that the boronic acid-caged Ir(III) complex is photochemically activatable to induce MMP loss and apoptosis under hypoxia.

Subsequently, the cytotoxicity of the iridium complex was investigated against lung carcinoma A549 by MTT assays (Table 1). In dark conditions, **IrBA** was found to be nontoxic to A549. In contrast, **IrNH$_2$** showed high dark cytotoxicity with IC_{50} values of 8.2 μM. When cancer cells treated by **IrBA** for 4 h were irradiated with 420 nm light for 10 min, the cytotoxicity was found to significantly increase with an IC_{50} of 1.0 μM, i.e., photo index (PI, $IC_{50,dark}/IC_{50,light}$) of >150. It is noteworthy that when the experiments were performed under hypoxia conditions (<0.1% O_2), **IrBA** also exhibited potent photocytotoxicity (4.4 μM) that is comparable to **IrNH$_2$** under dark conditions. Of note, the PI of **IrBA** under both normoxia and hypoxia are much stronger than **IrNH$_2$** under the same conditions. Similar results were found in breast adenocarcinoma (MCF-7) and melanoma (A375) cells (Table S1). For comparison, 5-ALA was inactive under hypoxia after light irradiation.

Then we examined if the PDT activity is involved in the cytotoxicity. Results showed that no superoxide and hydroxyl radicals were detected for **IrNH$_2$** and **IrBA** in A549 cells under normoxia and hypoxia conditions (Figure S12). In contrast, both **IrNH$_2$** and **IrBA** can generate $^1O_2$ with quantum yields of 0.50 and 0.46, respectively, under aerobic solution. When A549 cells were treated by **IrNH$_2$** under normoxia following light

Table 1. Photocytotoxicity (μM) of the Ir(III) Complexes toward A549 Cells under Normoxia and Hypoxia Conditions[a]

	IC_{50} under normoxia[b]			IC_{50} under hypoxia[c]		
Entry	Dark	Light	PI	Dark	Light	PI
IrBA	>150	1.0 ± 0.1	>150	>150	4.4 ± 0.3	>34
IrNH$_2$	8.2 ± 0.5	0.17 ± 0.03	48	9.0 ± 0.6	2 ± 0.4	4.5
5-ALA	>200	30.7 ± 2.0	>7	>200	>200	

[a]The cells were treated with compounds for 4 h and then irradiated with 420 nm light for 10 min. The cytotoxicity was measured after a total 48 h incubation. [b]Under normoxia. [c]Under hypoxia (O_2 < 0.1%). In all cases, the control group did not show obvious cytotoxicity under light irradiation.

https://doi.org/10.1021/jacs.3c00254
J. Am. Chem. Soc. 2023, 145, 10082−10091

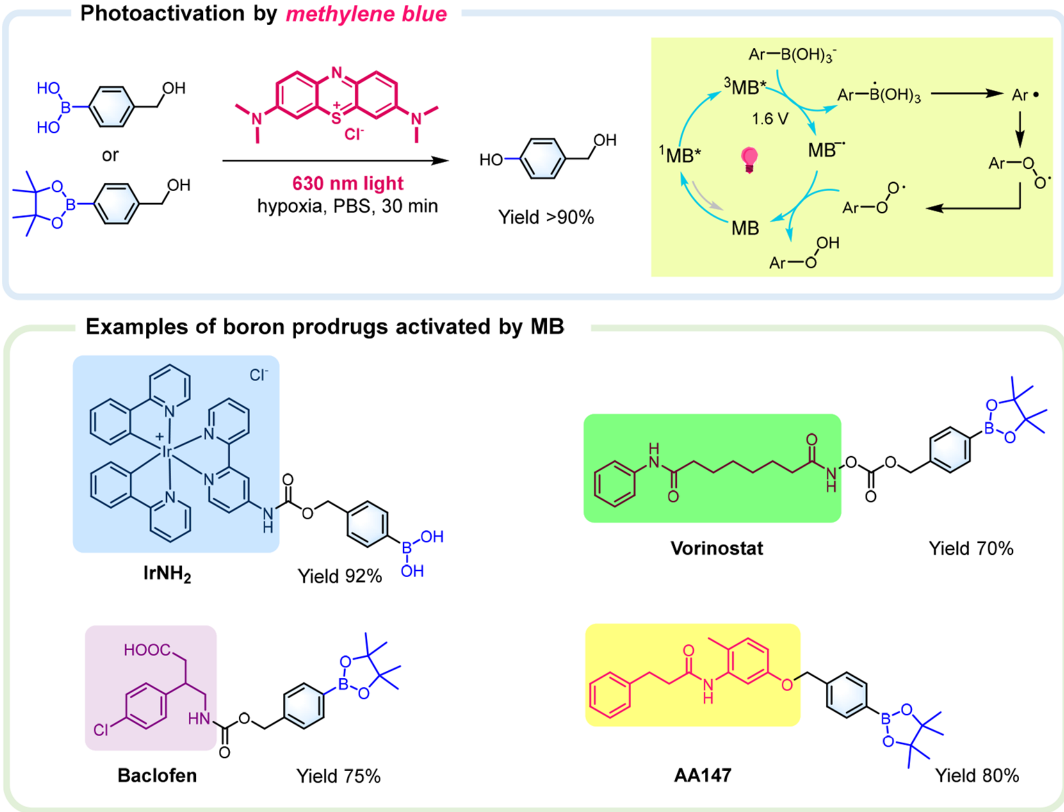

Figure 5. Activation of boronic acid/ester-caged compounds by MB after 30 min of 630 nm light irradiation at 1% O_2. The inset in the upper panel shows the photoactivation mechanism by MB. Examples of boronic acid/ester-caged prodrugs are shown in the lower panel with the parent drug highlighted.

irradiation, a significant amount of $^1O_2$ generation was found based on the SOSG probe (Figure S12), whereas **IrBA** formed a weaker signal. Under hypoxia, however, no $^1O_2$ signals were detected. Therefore, a type II PDT was involved in the photocytotoxicity under normoxia conditions (particularly for **IrNH$_2$**), but not under hypoxia.

Next, the photoactivity of **IrBA** was examined in 3D multicellular spheres (MCSs) that can mimic the pathophysiology of solid tumors including hypoxic regions.[89] When the A549 tumor spheroids reached ~500 μm in diameter, they were treated with each compound followed by calcein AM/ethidium homodimer (EthD-1) costaining. The probes can generate dual fluorescence and differentiate between living cells, which show green emission by the active esterase, and dead cells giving red emission due to a damaged cell membrane. As shown in Figure S13, in the group treated by **IrBA** (5 μM) for 24 h and a further 460 nm (23.9 mW/cm^2) light irradiation for 10 min, bright red fluorescence but negligible green emission were found. For comparison, in the photoirradiated group treated by 5-aminolevulinic acid (5-ALA), a clinic photosensitizer requiring O_2 for efficient PDT, or by **IrBA** without light irradiation, only green emission instead of red fluorescence was found, which again supports that photoirradiation can activate the anticancer activity of **IrBA** in tumor-like conditions.

The strong photocytotoxicity of **IrBA** particularly under hypoxia prompted us to further examine its in vivo antitumor activity in mice bearing A549 xenografts. In general, the tumor-bearing mice were injected (i.p.) with **IrBA** (2.5 mg/kg) once every 2 days with or without 460 nm light irradiation 4 h after each injection (on the localized tumor region). After 19 days of treatment, **IrBA** with light significantly suppressed tumor growth by 75% in tumor volume and 71% in tumor weight in comparison to the vehicle control (Figure S14). Of note, in the group of **IrBA** without light irradiation, little to low inhibition of tumor growth was found, indicating that the intratumoral reactive oxygen species (ROS) (H_2O_2) is unable to activate the boronic acid prodrug in this model. For the group treated with light only, no inhibition was found. Also, no mouse death or mouse body weight loss was observed during the whole treatment process.

Since certain photosensitizers are strong photo-oxidants and can absorb long-wavelength light, it is envisioned that they are applicable in activating boron prodrugs under hypoxia in a similar mechanism. A notable example is methylene blue (MB),[63] which has an intensive absorption at 600−700 nm and is a strong photo-oxidant (MB^*/MB^- = 1.6 V, vs SCE). Initially, a model compound, 4-(hydroxymethyl)phenylboronic acid, was tested by mixing with an equimolar ratio of MB followed by 630 nm light irradiation under hypoxia (O_2 = 1%), and 4-(hydroxymethyl)phenol was obtained in 96% yield (Figure S15a) within 30 min. A similar reaction yield of 91% was found when using boronic ester as the precursor (Figure S15b). Then, the ability of MB to activate **IrBA** was studied. After 30 min of 630 nm light irradiation under hypoxia (Figure 5), reaction yields of 92% (Figure S15c) were found to form **IrNH$_2$**. Such a reaction rate is faster than that by 10-fold excess of H_2O_2 and peroxynitrite generator SIN-1 requiring 3 and 1 h for full conversion, respectively (Figure S16). Similarly, boronic ester-caged baclofen (a clinic agonist of γ-aminobutyric acid receptor),[90] vorinostat (a clinic histone deacetylase inhibitor),[91] and AA147 (a preclinical activator

https://doi.org/10.1021/jacs.3c00254
J. Am. Chem. Soc. 2023, 145, 10082−10091

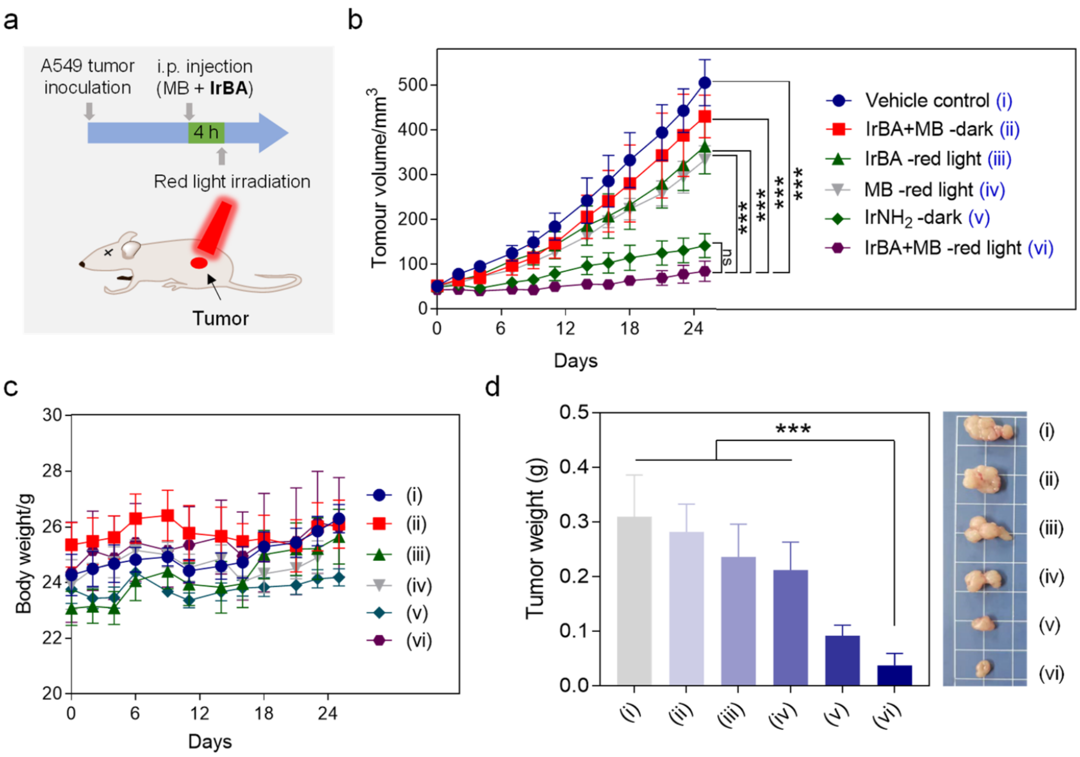

Figure 6. Red light-activated antitumor activity in mice bearing A549 tumor xenografts. The tumor-bearing mice were treated with "**IrBA** + MB", **IrBA**, or MB with or without 635 nm light irradiation once every 2 days for eight times (before day 16). The red light was given 4 h after each injection for 10 min. (a) Graphic description. (b−d) The tumor volume (b) and body weight (c) after different days of treatment are shown. The tumor weights after sacrificing the mice (day 25) were measured (d) with representative pictures shown. ***p < 0.001.

of ATF6 receptor)[92] can be activated with a 70−80% yield under similar photoactivation conditions (Figure S15d−f). In the control, when MB was replaced by fluorescein (FL), a photosensitizer that can reduce dioxygen but is unable to oxidize phenylborate anion ($[FL]^*/[FL]^-$ = 0.77 V, vs SCE),[93,94] no obvious reaction was found (even in the presence of NADH, data not shown), thus ruling out the mechanism involving $O_2^{\bullet-}$ for the photoinduced transformation reaction under hypoxia conditions.

Since MB can efficiently activate **IrBA** with a high efficiency in solution (Figure S17a), we further examined whether red light can activate **IrBA** in combination with MB in vitro and in vivo. Initially, the photocytotoxicity on 2D monolayer cells under hypoxia was tested. As depicted in Figure S17b and Table S2, while MB (2 μM) in 630 nm red light, **IrBA** in 630 nm light, and "**IrBA** + MB (2 μM)" in dark displayed weak cytotoxicity in hypoxia, the "**IrBA** + MB (2 μM)" combo under red light treatment potently suppressed cell growth with an IC_{50} of 3.6 to 13.6 μM (in terms of **IrBA** concentration), which is 15- to 20-fold stronger than that under dark conditions. When MB was used at 5 μM, a similar cytotoxicity profile was found (Figure S17c). Based on the Chou and Talalay method,[95] a good synergistic effect was observed (Figure S17d). The cytotoxicity of vorinostat-BA can be similarly activated by MB under 630 nm light irradiation (Figure S18, Table S3). On the other hand, in the A549 3D tumor spheroids (Figure S17e,f), the "**IrBA** (10 μM) + MB (2 μM)" combo treatment can also induce potent cytotoxicity after 630 nm light irradiation with full conversion into **IrNH$_2$**, but single treatment by **IrBA** or MB under the red light irradiation did not cause obvious cytotoxicity. We further examined the in vivo antitumor activity of the combo treatment. The mice bearing A549 tumor xenograft were treated (i.p.) by **IrBA** (2.5 mg/kg), MB (2 mg/kg), or "**IrBA** (2.5 mg/kg) + MB (2 mg/kg)" with or without 635 nm red light irradiation on the tumor region 4 h after each injection (Figure 6a). As shown in Figure 6b−d and Table S4, MB alone and **IrBA** alone mildly inhibited tumor growth by 33% and 28%, respectively, under red light irradiation after 25 days' treatment, and the "**IrBA** + MB" combo with red light irradiation significantly suppressed tumor growth by 83% (p < 0.001 compared to vehicle control), which is comparable to that by **IrNH$_2$** (2 mg/kg, equal molar to **IrBA**) treatment (72% inhibition). The treatment did not cause mouse death or body weight loss. Since the statistical significance in the "**IrBA** + MB-red light" group (vs vehicle control) can be found at day 4 (p < 0.01), the treatment dosage or frequency could be decreased in future animal studies.

■ CONCLUSION

In summary, we have identified a new photoactivation approach for boronic acid prodrugs. A proof-of-concept study by using a cyclometalated Ir(III) complex showed that this complex is photoactivatable under hypoxic conditions. The complex displays a reasonable stability under cellular conditions in the dark but can be efficiently and controllably activated by visible light irradiation. Mechanistic studies show that the activation process involves a photoinduced single electron transfer process to form a phenyl radical, which is extremely reactive to capture dioxygen at a rather low concentration. Consequently, the photoactivation process works particularly well in cancer cells under hypoxic conditions, accompanied by mitochondrial DNA damage, MMP loss, and strong cytotoxicity toward different cancer

https://doi.org/10.1021/jacs.3c00254
J. Am. Chem. Soc. 2023, 145, 10082−10091

cells. More importantly, while **IrBA** in the dark was unable to suppress tumor growth in vivo, the photoirradiation significantly increased the antitumor activity without causing obvious side effects. Since the intermolecular photoactivation by a clinic red light-absorbing methylene blue worked equally well under hypoxic conditions in vitro and in vivo, it is believed that the photoactivation approach could act as a general tool to highly spatiotemporally activate boron prodrugs for cancer eradication with high efficiency but limited side effects.

■ ASSOCIATED CONTENT

Supporting Information

The Supporting Information is available free of charge at https://pubs.acs.org/doi/10.1021/jacs.3c00254.

The experimental procedures for the chemical synthesis, characterization, photoreactions, cell-based biological experiments, and in vivo antitumor experiments (PDF)

■ AUTHOR INFORMATION

Corresponding Authors

Xiwen Xing − *Department of Biotechnology, College of Life Science and Technology, Jinan University, Guangzhou 510632, China*; Email: xingxiwen@jnu.edu.cn

Jong Seung Kim − *Department of Chemistry, Korea University, Seoul 02841, Korea*; orcid.org/0000-0003-3477-1172; Email: jongskim@korea.ac.kr

Taotao Zou − *Guangdong Key Laboratory of Chiral Molecule and Drug Discovery, School of Pharmaceutical Sciences, Sun Yat-Sen University, Guangzhou 510006, China*; orcid.org/0000-0001-9129-4398; Email: zoutt3@mail.sysu.edu.cn

Authors

Moyi Liu − *Guangdong Key Laboratory of Chiral Molecule and Drug Discovery, School of Pharmaceutical Sciences, Sun Yat-Sen University, Guangzhou 510006, China*

Yunli Luo − *Guangdong Key Laboratory of Chiral Molecule and Drug Discovery, School of Pharmaceutical Sciences, Sun Yat-Sen University, Guangzhou 510006, China*

Junyu Yan − *Guangdong Key Laboratory of Chiral Molecule and Drug Discovery, School of Pharmaceutical Sciences, Sun Yat-Sen University, Guangzhou 510006, China*

Xiaolin Xiong − *Guangdong Key Laboratory of Chiral Molecule and Drug Discovery, School of Pharmaceutical Sciences, Sun Yat-Sen University, Guangzhou 510006, China*

Complete contact information is available at: https://pubs.acs.org/10.1021/jacs.3c00254

Notes

The authors declare no competing financial interest.

■ ACKNOWLEDGMENTS

This work was financially supported by National Natural Science Foundation of China (No. 22122706), Guangdong Science and Technology Department (No. 2019QN01C125), Guangdong Basic and Applied Basic Research Foundation (No. 2021A1515012347), Guangzhou Science and Technology Projects (No. 202102020790), Guangdong Provincial Key Lab of Chiral Molecule and Drug Discovery (No. 2019B030301005), Key Laboratory of Bioinorganic and Synthetic Chemistry of Ministry of Education (Sun Yat-Sen University), National Key R&D Program of China (2022YFC2804101), and Outstanding Youth Project of Guangdong Natural Science Foundation (2022B1515020047).

■ REFERENCES

(1) Smoum, R.; Rubinstein, A.; Dembitsky, V. M.; Srebnik, M. Boron Containing Compounds as Protease Inhibitors. *Chem. Rev.* **2012**, *112*, 4156−4220.

(2) Diaz, D. B.; Yudin, A. K. The versatility of boron in biological target engagement. *Nat. Chem.* **2017**, *9*, 731−742.

(3) António, J. P. M.; Russo, R.; Carvalho, C. P.; Cal, P. M. S. D.; Gois, P. M. P. Boronic acids as building blocks for the construction of therapeutically useful bioconjugates. *Chem. Soc. Rev.* **2019**, *48*, 3513−3536.

(4) Baker, S. J.; Tomsho, J. W.; Benkovic, S. J. Boron-containing inhibitors of synthetases. *Chem. Soc. Rev.* **2011**, *40*, 4279−4285.

(5) Ellis, G. A.; Palte, M. J.; Raines, R. T. Boronate-Mediated Biologic Delivery. *J. Am. Chem. Soc.* **2012**, *134*, 3631−3634.

(6) Hashemzadeh, T.; Haghighatbin, M. A.; Agugiaro, J.; Wilson, D. J. D.; Hogan, C. F.; Barnard, P. J. Luminescent iridium(iii)-boronic acid complexes for carbohydrate sensing. *Dalton Trans.* **2020**, *49*, 11361−11374.

(7) Song, S.; Gao, P.; Sun, L.; Kang, D.; Kongsted, J.; Poongavanam, V.; Zhan, P.; Liu, X. Recent developments in the medicinal chemistry of single boron atom-containing compounds. *Acta Pharm. Sin. B* **2021**, *11*, 3035−3059.

(8) Trachootham, D.; Alexandre, J.; Huang, P. Targeting cancer cells by ROS-mediated mechanisms: a radical therapeutic approach? *Nat. Rev. Drug Discovery* **2009**, *8*, 579−591.

(9) Peiró Cadahía, J.; Previtali, V.; Troelsen, N. S.; Clausen, M. H. Prodrug strategies for targeted therapy triggered by reactive oxygen species. *MedChemComm* **2019**, *10*, 1531−1549.

(10) Maslah, H.; Skarbek, C.; Pethe, S.; Labruère, R. Anticancer boron-containing prodrugs responsive to oxidative stress from the tumor microenvironment. *Eur. J. Med. Chem.* **2020**, *207*, 112670.

(11) Wang, P.; Gong, Q.; Hu, J.; Li, X.; Zhang, X. Reactive Oxygen Species (ROS)-Responsive Prodrugs, Probes, and Theranostic Prodrugs: Applications in the ROS-Related Diseases. *J. Med. Chem.* **2021**, *64*, 298−325.

(12) Major Jourden, J. L.; Cohen, S. M. Hydrogen Peroxide Activated Matrix Metalloproteinase Inhibitors: A Prodrug Approach. *Angew. Chem., Int. Ed.* **2010**, *49*, 6795−6797.

(13) Kuang, Y.; Balakrishnan, K.; Gandhi, V.; Peng, X. Hydrogen Peroxide Inducible DNA Cross-Linking Agents: Targeted Anticancer Prodrugs. *J. Am. Chem. Soc.* **2011**, *133*, 19278−19281.

(14) Hagen, H.; Marzenell, P.; Jentzsch, E.; Wenz, F.; Veldwijk, M. R.; Mokhir, A. Aminoferrocene-Based Prodrugs Activated by Reactive Oxygen Species. *J. Med. Chem.* **2012**, *55*, 924−934.

(15) Marzenell, P.; Hagen, H.; Sellner, L.; Zenz, T.; Grinyte, R.; Pavlov, V.; Daum, S.; Mokhir, A. Aminoferrocene-Based Prodrugs and Their Effects on Human Normal and Cancer Cells as Well as Bacterial Cells. *J. Med. Chem.* **2013**, *56*, 6935−6944.

(16) Kim, E.-J.; Bhuniya, S.; Lee, H.; Kim, H. M.; Cheong, C.; Maiti, S.; Hong, K. S.; Kim, J. S. An Activatable Prodrug for the Treatment of Metastatic Tumors. *J. Am. Chem. Soc.* **2014**, *136*, 13888−13894.

(17) Kumar, R.; Han, J.; Lim, H.-J.; Ren, W. X.; Lim, J.-Y.; Kim, J.-H.; Kim, J. S. Mitochondrial Induced and Self-Monitored Intrinsic Apoptosis by Antitumor Theranostic Prodrug: In Vivo Imaging and Precise Cancer Treatment. *J. Am. Chem. Soc.* **2014**, *136*, 17836−17843.

(18) Wang, M.; Sun, S.; Neufeld, C. I.; Perez-Ramirez, B.; Xu, Q. Reactive Oxygen Species-Responsive Protein Modification and Its Intracellular Delivery for Targeted Cancer Therapy. *Angew. Chem., Int. Ed.* **2014**, *53*, 13444−13448.

(19) Daum, S.; Chekhun, V. F.; Todor, I. N.; Lukianova, N. Y.; Shvets, Y. V.; Sellner, L.; Putzker, K.; Lewis, J.; Zenz, T.; de Graaf, I. A. M.; Groothuis, G. M. M.; Casini, A.; Zozulia, O.; Hampel, F.; Mokhir, A. Improved Synthesis of N-Benzylaminoferrocene-Based Prodrugs and Evaluation of Their Toxicity and Antileukemic Activity. *J. Med. Chem.* **2015**, *58*, 2015−2024.

(20) Hanna, R. D.; Naro, Y.; Deiters, A.; Floreancig, P. E. Alcohol, Aldehyde, and Ketone Liberation and Intracellular Cargo Release through Peroxide-Mediated α-Boryl Ether Fragmentation. *J. Am. Chem. Soc.* **2016**, *138*, 13353−13360.
(21) Reshetnikov, V.; Daum, S.; Mokhir, A. Cancer-Specific, Intracellular, Reductive Activation of Anticancer PtIV Prodrugs. *Chem.—Eur. J.* **2017**, *23*, 5678−5681.
(22) Hoang, T. T.; Smith, T. P.; Raines, R. T. A Boronic Acid Conjugate of Angiogenin that Shows ROS-Responsive Neuroprotective Activity. *Angew. Chem., Int. Ed.* **2017**, *56*, 2619−2622.
(23) Chen, W.; Fan, H.; Balakrishnan, K.; Wang, Y.; Sun, H.; Fan, Y.; Gandhi, V.; Arnold, L. A.; Peng, X. Discovery and Optimization of Novel Hydrogen Peroxide Activated Aromatic Nitrogen Mustard Derivatives as Highly Potent Anticancer Agents. *J. Med. Chem.* **2018**, *61*, 9132−9145.
(24) Xiang, H.; Wu, Y.; Zhu, X.; She, M.; An, Q.; Zhou, R.; Xu, P.; Zhao, F.; Yan, L.; Zhao, Y. Highly Stable Silica-Coated Bismuth Nanoparticles Deliver Tumor Microenvironment-Responsive Prodrugs to Enhance Tumor-Specific Photoradiotherapy. *J. Am. Chem. Soc.* **2021**, *143*, 11449−11461.
(25) Liao, X.; Shen, J.; Wu, W.; Kuang, S.; Lin, M.; Karges, J.; Tang, Z.; Chao, H. A mitochondrial-targeting iridium(iii) complex for H_2O_2-responsive and oxidative stress amplified two-photon photodynamic therapy. *Inorg. Chem. Front.* **2021**, *8*, 5045−5053.
(26) Maslah, H.; Skarbek, C.; Gourson, C.; Plamont, M.-A.; Pethe, S.; Jullien, L.; Le Saux, T.; Labruère, R. In-Cell Generation of Anticancer Phenanthridine Through Bioorthogonal Cyclization in Antitumor Prodrug Development. *Angew. Chem., Int. Ed.* **2021**, *60*, 24043−24047.
(27) Ertl, P.; Altmann, E.; McKenna, J. M. The Most Common Functional Groups in Bioactive Molecules and How Their Popularity Has Evolved over Time. *J. Med. Chem.* **2020**, *63*, 8408−8418.
(28) Graham, B. J.; Windsor, I. W.; Gold, B.; Raines, R. T. Boronic acid with high oxidative stability and utility in biological contexts. *Proc. Natl. Acad. Sci. U. S. A.* **2021**, *118*, No. e2013691118.
(29) Daum, S.; Reshetnikov, M. S. V.; Sisa, M.; Dumych, T.; Lootsik, M. D.; Bilyy, R.; Bila, E.; Janko, C.; Alexiou, C.; Herrmann, M.; Sellner, L.; Mokhir, A. Lysosome-Targeting Amplifiers of Reactive Oxygen Species as Anticancer Prodrugs. *Angew. Chem., Int. Ed.* **2017**, *56*, 15545−15549.
(30) Noh, J.; Kwon, B.; Han, E.; Park, M.; Yang, W.; Cho, W.; Yoo, W.; Khang, G.; Lee, D. Amplification of oxidative stress by a dual stimuli-responsive hybrid drug enhances cancer cell death. *Nat. Commun.* **2015**, *6*, 6907.
(31) Reshetnikov, V.; Daum, S.; Janko, C.; Karawacka, W.; Tietze, R.; Alexiou, C.; Paryzhak, S.; Dumych, T.; Bilyy, R.; Tripal, P.; Schmid, B.; Palmisano, R.; Mokhir, A. ROS-Responsive N-Alkylaminoferrocenes for Cancer-Cell-Specific Targeting of Mitochondria. *Angew. Chem., Int. Ed.* **2018**, *57*, 11943−11946.
(32) Pan, Q.; Zhang, B.; Peng, X.; Wan, S.; Luo, K.; Gao, W.; Pu, Y.; He, B. A dithiocarbamate-based H2O2-responsive prodrug for combinational chemotherapy and oxidative stress amplification therapy. *Chem. Commun.* **2019**, *55*, 13896−13899.
(33) Xu, H.-G.; Schikora, M.; Sisa, M.; Daum, S.; Klemt, I.; Janko, C.; Alexiou, C.; Bila, G.; Bilyy, R.; Gong, W.; Schmitt, M.; Sellner, L.; Mokhir, A. An Endoplasmic Reticulum Specific Pro-amplifier of Reactive Oxygen Species in Cancer Cells. *Angew. Chem., Int. Ed.* **2021**, *60*, 11158−11162.
(34) Joshi, T.; Pierroz, V.; Mari, C.; Gemperle, L.; Ferrari, S.; Gasser, G. A Bis(dipyridophenazine)(2-(2-pyridyl)pyrimidine-4-carboxylic acid)ruthenium(II) Complex with Anticancer Action upon Photodeprotection. *Angew. Chem., Int. Ed.* **2014**, *53*, 2960−2963.
(35) Imberti, C.; Zhang, P.; Huang, H.; Sadler, P. J. New designs for phototherapeutic transition metal complexes. *Angew. Chem., Int. Ed.* **2020**, *59*, 61−73.
(36) Shi, H.; Sadler, P. J. How promising is phototherapy for cancer? *Br. J. Cancer* **2020**, *123*, 871−873.
(37) Shi, H.; Sadler, P. J. Photoactive metallodrugs. In *Reference Module in Chemistry, Molecular Sciences and Chemical Engineering*; Elsevier, 2021.
(38) Zhang, K. Y.; Gao, P.; Sun, G.; Zhang, T.; Li, X.; Liu, S.; Zhao, Q.; Lo, K. K.-W.; Huang, W. Dual-Phosphorescent Iridium(III) Complexes Extending Oxygen Sensing from Hypoxia to Hyperoxia. *J. Am. Chem. Soc.* **2018**, *140*, 7827−7834.
(39) Wang, X.; Wang, X.; Jin, S.; Muhammad, N.; Guo, Z. Stimuli-Responsive Therapeutic Metallodrugs. *Chem. Rev.* **2019**, *119*, 1138−1192.
(40) Müller, P.; Schroder, B.; Parkinson, J. A.; Kratochwil, N. A.; Coxall, R. A.; Parkin, A.; Parsons, S.; Sadler, P. J. Nucleotide Cross-Linking Induced by Photoreactions of Platinum(IV)-Azide Complexes. *Angew. Chem., Int. Ed.* **2003**, *42*, 335−339.
(41) Farrer, N. J.; Woods, J. A.; Salassa, L.; Zhao, Y.; Robinson, K. S.; Clarkson, G.; Mackay, F. S.; Sadler, P. J. A Potent Trans-Diimine Platinum Anticancer Complex Photoactivated by Visible Light. *Angew. Chem., Int. Ed.* **2010**, *49*, 8905−8908.
(42) Butler, J. S.; Woods, J. A.; Farrer, N. J.; Newton, M. E.; Sadler, P. J. Tryptophan Switch for a Photoactivated Platinum Anticancer Complex. *J. Am. Chem. Soc.* **2012**, *134*, 16508−16511.
(43) Alonso-de Castro, S.; Ruggiero, E.; Ruiz-de-Angulo, A.; Rezabal, E.; Mareque-Rivas, J. C.; Lopez, X.; López-Gallego, F.; Salassa, L. Riboflavin as a bioorthogonal photocatalyst for the activation of a Pt^{IV} prodrug. *Chem. Sci.* **2017**, *8*, 4619−4625.
(44) Farrer, N. J.; Sharma, G.; Sayers, R.; Shaili, E.; Sadler, P. J. Platinum(iv) azido complexes undergo copper-free click reactions with alkynes. *Dalton Trans.* **2018**, *47*, 10553−10560.
(45) Alonso-de Castro, S.; Cortajarena, A. L.; López-Gallego, F.; Salassa, L. Bioorthogonal Catalytic Activation of Platinum and Ruthenium Anticancer Complexes by FAD and Flavoproteins. *Angew. Chem., Int. Ed.* **2018**, *57*, 3143−3147.
(46) Bolitho, E. M.; Sanchez-Cano, C.; Shi, H.; Quinn, P. D.; Harkiolaki, M.; Imberti, C.; Sadler, P. J. Single-Cell Chemistry of Photoactivatable Platinum Anticancer Complexes. *J. Am. Chem. Soc.* **2021**, *143*, 20224−20240.
(47) Velasco-Lozano, S.; Castro, S. A.-d.; Sanchez-Cano, C.; Benítez-Mateos, A. I.; López-Gallego, F.; Salassa, L. Metal substrate catalysis in the confined space for platinum drug delivery. *Chem. Sci.* **2021**, *13*, 59−67.
(48) Askes, S. H. C.; Bahreman, A.; Bonnet, S. Activation of a Photodissociative Ruthenium Complex by Triplet-Triplet Annihilation Upconversion in Liposomes. *Angew. Chem., Int. Ed.* **2014**, *53*, 1029−1033.
(49) Bonnet, S. Why develop photoactivated chemotherapy? *Dalton Trans.* **2018**, *47*, 10330−10343.
(50) Lameijer, L. N.; Ernst, D.; Hopkins, S. L.; Meijer, M. S.; Askes, S. H. C.; Le Dévédec, S. E.; Bonnet, S. A Red-Light-Activated Ruthenium-Caged NAMPT Inhibitor Remains Phototoxic in Hypoxic Cancer Cells. *Angew. Chem., Int. Ed.* **2017**, *56*, 11549−11553.
(51) Li, A.; Turro, C.; Kodanko, J. J. Ru(ii) polypyridyl complexes as photocages for bioactive compounds containing nitriles and aromatic heterocycles. *Chem. Commun.* **2018**, *54*, 1280−1290.
(52) van Rixel, V. H. S.; Busemann, A.; Wissingh, M. F.; Hopkins, S. L.; Siewert, B.; van de Griend, C.; Siegler, M. A.; Marzo, T.; Papi, F.; Ferraroni, M.; Gratteri, P.; Bazzicalupi, C.; Messori, L.; Bonnet, S. Induction of a four-way junction structure in the DNA palindromic hexanucleotide 5′-d(CGTACG)-3′ by a mononuclear platinum complex. *Angew. Chem., Int. Ed.* **2019**, *58*, 9378−9382.
(53) van Rixel, V. H. S.; Ramu, V.; Auyeung, A. B.; Beztsinna, N.; Leger, D. Y.; Lameijer, L. N.; Hilt, S. T.; Le Dévédec, S. E.; Yildiz, T.; Betancourt, T.; Gildner, M. B.; Hudnall, T. W.; Sol, V.; Liagre, B.; Kornienko, A.; Bonnet, S. Photo-Uncaging of a Microtubule-Targeted Rigidin Analogue in Hypoxic Cancer Cells and in a Xenograft Mouse Model. *J. Am. Chem. Soc.* **2019**, *141*, 18444−18454.
(54) Toupin, N.; Steinke, S. J.; Nadella, S.; Li, A.; Rohrabaugh, T. N.; Samuels, E. R.; Turro, C.; Sevrioukova, I. F.; Kodanko, J. J. Photosensitive Ru(II) Complexes as Inhibitors of the Major Human

https://doi.org/10.1021/jacs.3c00254
J. Am. Chem. Soc. 2023, 145, 10082−10091

Drug Metabolizing Enzyme CYP3A4. *J. Am. Chem. Soc.* **2021**, *143*, 9191−9205.
(55) Steinke, S. J.; Gupta, S.; Piechota, E. J.; Moore, C. E.; Kodanko, J. J.; Turro, C. Photocytotoxicity and photoinduced phosphine ligand exchange in a Ru(ii) polypyridyl complex. *Chem. Sci.* **2022**, *13*, 1933−1945.
(56) Kastl, A.; Wilbuer, A.; Merkel, A. L.; Feng, L.; Di Fazio, P.; Ocker, M.; Meggers, E. Dual anticancer activity in a single compound: visible-light-induced apoptosis by an antiangiogenic iridium complex. *Chem. Commun.* **2012**, *48*, 1863−1865.
(57) Bahreman, A.; Cuello-Garibo, J.-A.; Bonnet, S. Yellow-light sensitization of a ligand photosubstitution reaction in a ruthenium polypyridyl complex covalently bound to a rhodamine dye. *Dalton Trans.* **2014**, *43*, 4494−4505.
(58) Leonidova, A.; Pierroz, V.; Rubbiani, R.; Lan, Y.; Schmitz, A. G.; Kaech, A.; Sigel, R. K. O.; Ferrari, S.; Gasser, G. Photo-induced uncaging of a specific Re(i) organometallic complex in living cells. *Chem. Sci.* **2014**, *5*, 4044−4056.
(59) Li, Z.; David, A.; Albani, B. A.; Pellois, J.-P.; Turro, C.; Dunbar, K. R. Optimizing the Electronic Properties of Photoactive Anticancer Oxypyridine-Bridged Dirhodium(II,II) Complexes. *J. Am. Chem. Soc.* **2014**, *136*, 17058−17070.
(60) Garai, A.; Pant, I.; Banerjee, S.; Banik, B.; Kondaiah, P.; Chakravarty, A. R. Photorelease and Cellular Delivery of Mitocurcumin from Its Cytotoxic Cobalt(III) Complex in Visible Light. *Inorg. Chem.* **2016**, *55*, 6027−6035.
(61) Askes, S. H. C.; Reddy, G. U.; Wyrwa, R.; Bonnet, S.; Schiller, A. Red Light-Triggered CO Release from $Mn_2(CO)_{10}$ Using Triplet Sensitization in Polymer Nonwoven Fabrics. *J. Am. Chem. Soc.* **2017**, *139*, 15292−15295.
(62) Luo, H.; Cao, B.; Chan, A. S. C.; Sun, R. W.-Y.; Zou, T. Cyclometalated Gold(III)-Hydride Complexes Exhibit Visible Light-Induced Thiol Reactivity and Act as Potent Photo-Activated Anti-Cancer Agents. *Angew. Chem., Int. Ed.* **2020**, *59*, 11046−11052.
(63) Pitre, S. P.; McTiernan, C. D.; Ismaili, H.; Scaiano, J. C. Mechanistic Insights and Kinetic Analysis for the Oxidative Hydroxylation of Arylboronic Acids by Visible Light Photoredox Catalysis: A Metal-Free Alternative. *J. Am. Chem. Soc.* **2013**, *135*, 13286−13289.
(64) Wang, H.; Li, W.-G.; Zeng, K.; Wu, Y.-J.; Zhang, Y.; Xu, T.-L.; Chen, Y. Photocatalysis Enables Visible-Light Uncaging of Bioactive Molecules in Live Cells. *Angew. Chem., Int. Ed.* **2019**, *58*, 561−565.
(65) Sharma, A.; Arambula, J. F.; Koo, S.; Kumar, R.; Singh, H.; Sessler, J. L.; Kim, J. S. Hypoxia-targeted drug delivery. *Chem. Soc. Rev.* **2019**, *48*, 771−813.
(66) Maillard, B.; Ingold, K. U.; Scaiano, J. C. Rate constants for the reactions of free radicals with oxygen in solution. *J. Am. Chem. Soc.* **1983**, *105*, 5095−5099.
(67) Sommeling, P. M.; Mulder, P.; Louw, R.; Avila, D. V.; Lusztyk, J.; Ingold, K. U. Rate of reaction of phenyl radicals with oxygen in solution and in the gas phase. *J. Phys. Chem.* **1993**, *97*, 8361−8364.
(68) Iwata, Y.; Tanaka, Y.; Kubosaki, S.; Morita, T.; Yoshimi, Y. A strategy for generating aryl radicals from arylborates through organic photoredox catalysis: photo-Meerwein type arylation of electron-deficient alkenes. *Chem. Commun.* **2018**, *54*, 1257−1260.
(69) Chilamari, M.; Immel, J. R.; Bloom, S. General Access to C-Centered Radicals: Combining a Bioinspired Photocatalyst with Boronic Acids in Aqueous Media. *ACS Catal.* **2020**, *10*, 12727−12737.
(70) Yao, Q.; Fan, J.; Long, S.; Zhao, X.; Li, H.; Du, J.; Shao, K.; Peng, X. The concept and examples of type-III photosensitizers for cancer photodynamic therapy. *Chem.* **2022**, *8*, 197−209.
(71) Lo, K. K.-W.; Chung, C.-K.; Lee, T. K.-M.; Lui, L.-H.; Tsang, K. H.-K.; Zhu, N. New Luminescent Cyclometalated Iridium(III) Diimine Complexes as Biological Labeling Reagents. *Inorg. Chem.* **2003**, *42*, 6886−6897.
(72) Ma, D.-L.; Chan, D. S.-H.; Leung, C.-H. Group 9 Organometallic Compounds for Therapeutic and Bioanalytical Applications. *Acc. Chem. Res.* **2014**, *47*, 3614−3631.
(73) Liu, Z.; Sadler, P. J. Organoiridium Complexes: Anticancer Agents and Catalysts. *Acc. Chem. Res.* **2014**, *47*, 1174−1185.
(74) Lo, K. K.-W. Luminescent Rhenium(I) and Iridium(III) Polypyridine Complexes as Biological Probes, Imaging Reagents, and Photocytotoxic Agents. *Acc. Chem. Res.* **2015**, *48*, 2985−2995.
(75) Lee, L. C.-C.; Lau, J. C.-W.; Liu, H.-W.; Lo, K. K.-W. Conferring Phosphorogenic Properties on Iridium(III)-based Bioorthogonal Probes through the Modification with a Nitrone Unit. *Angew. Chem., Int. Ed.* **2016**, *55*, 1046−1049.
(76) Meggers, E. Exploiting Octahedral Stereocenters: From Enzyme Inhibition to Asymmetric Photoredox Catalysis. *Angew. Chem., Int. Ed.* **2017**, *56*, 5668−5675.
(77) Novohradsky, V.; Rovira, A.; Hally, C.; Galindo, A.; Vigueras, G.; Gandioso, A.; Svitelova, M.; Bresolí-Obach, R.; Kostrhunova, H.; Markova, L.; Kasparkova, J.; Nonell, S.; Ruiz, J.; Brabec, V.; Marchán, V. Towards Novel Photodynamic Anticancer Agents Generating Superoxide Anion Radicals: A Cyclometalated Ir^{III} Complex Conjugated to a Far-Red Emitting Coumarin. *Angew. Chem., Int. Ed.* **2019**, *58*, 6311−6315.
(78) Bevernaegie, R.; Doix, B.; Bastien, E.; Diman, A.; Decottignies, A.; Feron, O.; Elias, B. Exploring the Phototoxicity of Hypoxic Active Iridium(III)-Based Sensitizers in 3D Tumor Spheroids. *J. Am. Chem. Soc.* **2019**, *141*, 18486−18491.
(79) Huang, H.; Banerjee, S.; Qiu, K.; Zhang, P.; Blacque, O.; Malcomson, T.; Paterson, M. J.; Clarkson, G. J.; Staniforth, M.; Stavros, V. G.; Gasser, G.; Chao, H.; Sadler, P. J. Targeted photoredox catalysis in cancer cells. *Nat. Chem.* **2019**, *11*, 1041−1048.
(80) Boros, E.; Dyson, P. J.; Gasser, G. Classification of Metal-Based Drugs according to Their Mechanisms of Action. *Chem.* **2020**, *6*, 41−60.
(81) McFarland, S. A.; Mandel, A.; Dumoulin-White, R.; Gasser, G. Metal-based photosensitizers for photodynamic therapy: the future of multimodal oncology? *Curr. Opin. Chem. Biol.* **2020**, *56*, 23−27.
(82) Yip, A. M.-H.; Lai, C. K.-H.; Yiu, K. S.-M.; Lo, K. K.-W. Phosphorogenic Iridium(III) bis-Tetrazine Complexes for Bioorthogonal Peptide Stapling, Bioimaging, Photocytotoxic Applications, and the Construction of Nanosized Hydrogels. *Angew. Chem., Int. Ed.* **2022**, *61*, No. e202116078.
(83) Suzuki, J.; Shida, N.; Inagi, S.; Fuchigami, T. Electrochemical Properties and Reactions of Organoboronic Acids in the Presence of Fluoride Ions. *Electroanalysis* **2016**, *28*, 2797−2801.
(84) Augusto, O. Alkylation and cleavage of DNA by carbon-centered radical metabolites. *Free Radical Biol. Med.* **1993**, *15*, 329−336.
(85) Hypoxic bags were used in this work to create the hypoxic oxygen atmosphere.
(86) Bai, R.-K.; Wong, L.-J. C. Simultaneous Detection and Quantification of Mitochondrial DNA Deletion(s), Depletion, and Over-Replication in Patients with Mitochondrial Disease. *J. Mol. Diagn.* **2005**, *7*, 613−622.
(87) Venegas, V.; Wang, J.; Dimmock, D.; Wong, L.-J. Real-Time Quantitative PCR Analysis of Mitochondrial DNA Content. *Curr. Protoc. Hum. Genet.* **2011**, *68*, 19.7.1−19.7.12.
(88) McCue, A. C.; Moreau, W. M.; Shell, T. A. Visible Light-Induced Radical Mediated DNA Damage. *Photochem. Photobiol.* **2018**, *94*, 545−551.
(89) Riffle, S.; Pandey, R. N.; Albert, M.; Hegde, R. S. Linking hypoxia, DNA damage and proliferation in multicellular tumor spheroids. *BMC Cancer* **2017**, *17*, 338.
(90) Cousins, M. S.; Roberts, D. C. S.; Wit, H. d. GABAB receptor agonists for the treatment of drug addiction: a review of recent findings. *Drug Alcohol Depend.* **2002**, *65*, 209−220.
(91) Marks, P. A.; Breslow, R. Dimethyl sulfoxide to vorinostat: development of this histone deacetylase inhibitor as an anticancer drug. *Nat. Biotechnol.* **2007**, *25*, 84−90.
(92) Almasy, K. M.; Davies, J. P.; Lisy, S. M.; Tirgar, R.; Tran, S. C.; Plate, L. Small-molecule endoplasmic reticulum proteostasis regulator acts as a broad-spectrum inhibitor of dengue and Zika virus infections. *Proc. Natl. Acad. Sci. U. S. A.* **2021**, *118*, No. e2012209118.

(93) Romero, N. A.; Nicewicz, D. A. Organic Photoredox Catalysis. *Chem. Rev.* **2016**, *116*, 10075−10166.
(94) Shen, T.; Zhao, Z.-G.; Yu, Q.; Xu, H.-J. Photosensitized reduction of benzil by heteroatom-containing anthracene dyes. *J. Photochem. Photobiol., A* **1989**, *47*, 203−212.
(95) Chou, T.-C. Drug Combination Studies and Their Synergy Quantification Using the Chou-Talalay Method. *Cancer Res.* **2010**, *70*, 440−446.

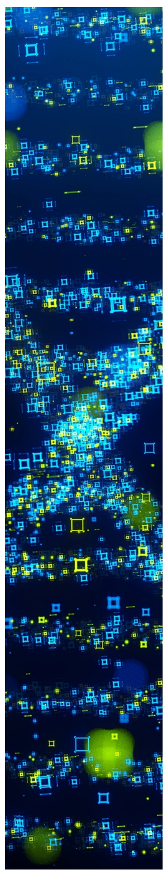

https://doi.org/10.1021/jacs.3c00254
J. Am. Chem. Soc. 2023, 145, 10082−10091